Digital Elevation Model Aided SAR-based GMTI Processing in Urban Environments

Digital Elevation Model Aided SAR-based GMTI Processing in Urban Environments

Di Wu, Mehrdad Yaghoobi and Mike Davies
School of Engineering
University of Edinburgh
UK, EH9 3JL
Email: {D.Wu, m.yaghoobi-vaighan, mike.davies}@ed.ac.uk

***Abstract*—This paper presents a work for imaging the moving targets and estimating their velocities with better accuracies using the Digital Elevation Map (DEM) in urban environments under multi-channel Synthetic Aperture Radar (SAR) scenarios. Given the received phase histories pre-processed by channel balancing techniques, we employ Ground Moving Target Indicator (GMTI) methods to detect the moving targets, and apply the DEM to assist imaging the observed scene and estimating the states of the targets. Specifically the DEM can be leveraged to calibrate the positions of the moving targets and give further constraints on the estimations of velocities. The described work is demonstrated through the AFRL Gotcha challenge data. We present the positions of the relocated targets along with their velocity estimations as the experimental results.**

***Index Terms*—SAR, GMTI, digital elevation map**

I. Introduction

SAR was originally developed as a flexible sensing technique to produce high resolution images of the observed scene for surveillance purposes. In particular, SAR-based GMTI aims to indicate the moving targets within SAR images and estimate the moving target parameters including their physical positions and velocities. The developments on GMTI techniques in the last decade significantly captured the attention from the SAR community due to its capabilities in promoting situational awareness. In practice, SAR imaging assumes that the observed scene contains only static targets. Therefore, moving targets will introduce blurrings and displacements to the SAR images, and they need to be relocated and refocused using GMTI techniques.

Within the multi-channel SAR framework, widely used GMTI techniques include Displaced Phase Center Antenna (DPCA), Along Track Interferometry (ATI) and Space-time Adaptive Processing (STAP) [1][2][3]. DPCA and ATI are subtractive methods which suppress the clutter and reveal the moving targets with magnitudes and interference phases respectively. STAP can be taken as the extended version of DPCA and it is well known to be computationally expensive. Take the ATI as an example, radial velocities of the moving targets can be estimated and the moving targets can then be relocated accordingly. However, in particular scenarios where the monitored region has significant variations on elevations, the localisations of the targets will be distorted and inconsistencies will show up if we compare the relocated targets to the ground truth target path.

In this paper, we discuss how the DEM can be utilised to enhance the relocations of the moving targets and improve the estimations of targets' states. The remainder of the paper is organized as follows. Section two describes the signal modeling of a standard multi-channel SAR system with a specific terrain map. In section three, the DEM aided SAR/GMTI processings are presented. We first introduce the SAR basics and GMTI approaches. Then we focus on incorporating the DEM into the moving target imaging and the target states estimations. In section four, we demonstrate the performance of the proposed methods using the real airborne SAR data. Conclusions are presented in section five.

II. Signal Modeling

In Fig. 1 we depict a standard multi-channel SAR system in the spotlight mode with a number of moving targets in the observed scene. A terrain map is associated with the monitored region. The phase centres of antennas are equally spaced with a distance d along the flight path of the platform. Let the azimuth time (slow time) of the transmitted pulses be τ_n where $n = \{1, 2, ..., N\}$ is the pulse number; $\mathbf{r}(\tau_n)$ be the instantaneous spatial position of one target at τ_n; $r_i^{(t)}(\tau_n)$ and $r_i^{(o)}(\tau_n)$ denote the distance from the target to the $i-$th antenna and the distance from the scene origin to the corresponding antenna position respectively. Within a short sub-aperture, we can assume that the platform velocity is a constant v_p.

For the target at $\mathbf{r}(\tau_n)$, the discrete received phase histories from the $i-$th channel after the de-chirping process (the movement of the platform is compensated with reference to the scene origin) can be formulated as:

$$Y_i(f_k, \tau_n) = A_i \sigma(\mathbf{r}(\tau_n)) \exp\left(-\frac{j4\pi f_k u_i(\tau_n)}{c}\right) \qquad (1)$$

where $\{f_k | k = 1, 2, ..., K\}$ denotes the range frequencies; A_i represents a nominal factor which accounts for the beam pattern and energy loss for the $i-$th channel; $\sigma(\mathbf{r}(\tau_n))$ is the complex reflectivity of the target at $\mathbf{r}(\tau_n)$; c is the speed of light and $u_i(\tau_n)$ is the differential range $r_i^{(t)}(\tau_n) - r_i^{(o)}(\tau_n)$. Given that we have multiple targets in the observed scene, the received data can be assembled by accumulating the received signals from all the targets. Thus, the received data can be further reformulated in the matrix-vector form as

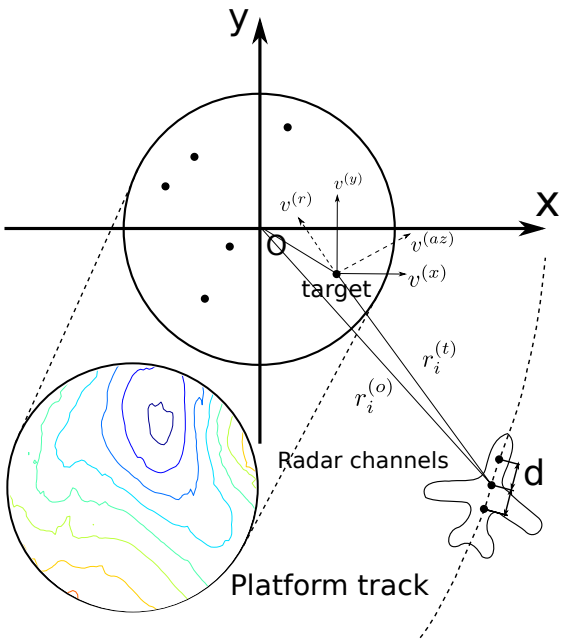

Fig. 1. The geometry of a multi-channel SAR system with moving targets in the monitored scene which is associated with a terrain map.

$\mathbf{Y}_i = \Phi_F(\mathbf{X})$, where Φ_F is the forward projection operator to map the image domain to the data domain and $\mathbf{X} \in \mathbb{C}^{M\times L}$ denotes the collection of the target reflectivities.

III. Digital Elevation Model Aided SAR/GMTI

Based on the described multi-channel SAR system we focus on the DEM aided SAR/GMTI processings in this section. How the terrain information can help locate the moving targets and estimate their states will be discussed in details.

A. SAR Pre-processing

Given that the phase histories have been range compressed and range-migration corrected, it has been reported that for two channels the signals in Doppler and range-frequency domain can be approximated with the equations [4]:

$$\begin{aligned} Y_1(\omega,\Omega) &\cong c(\omega)h_1(\Omega)D_1(q(\omega)) \\ Y_2(\omega,\Omega) &\cong c(\omega)h_2(\Omega)D_2(q(\omega))exp(-j\frac{d}{2v_p}\omega) \end{aligned} \tag{2}$$

where $c(\omega)$ is the nominal factor to denote the complex Doppler dependencies, $h_i(\Omega)$ is the transfer function with the range frequency Ω for the $i-$th channel, D_i is the antenna pattern for the $i-$th channel, and $q(\omega)$ is the directional cosine history over the Doppler frequency ω.

From (2) it is shown that the phase histories can be balanced with two functions in azimuth and range directions respectively, i.e. $H_{az}(\omega)$ and $H_{rg}(\Omega)$ in (3), to retrieve the same responses for stationary targets between different channels.

$$\begin{aligned} H_{az}(\omega) &= \frac{D_1(q(\omega))}{D_2(q(\omega))exp(-j\frac{d}{2v_p}\omega)} \\ H_{rg}(\Omega) &= \frac{h_1(\Omega)}{h_2(\Omega)} \end{aligned} \tag{3}$$

This process is especially crucial for subtractive GMTI methods such as DPCA and ATI which reveal moving targets in SAR images through the differences between channels. Specifically the phase history for the second channel can be balanced via $\widetilde{\mathbf{Y}}_2(\omega,\Omega) = \mathbf{Y}_2(\omega,\Omega)H_{az}(\omega)H_{rg}(\Omega)$. An adaptive 2D channel balancing technique was proposed to update $H_{az}(\omega)$ and $H_{rg}(\Omega)$ with iterations [4]. We will employ this approach to pre-process the SAR data in the remainder of the paper.

In practice, we tend to employ more azimuth samples to better mitigate the imperfect balances along the range direction. However, $H_{az}(\omega)$ have strong degradations in amplitudes among azimuth frequencies, and this will induce less calibration accuracies for the azimuth samples in high frequencies. The simple solution is to estimate $H_{az}(\omega)$ and $H_{rg}(\Omega)$ with a number of azimuth samples and preserve only the low frequencies in $H_{az}(\omega)$.

B. SAR Imaging and GMTI

The SAR imaging process can be interpreted as approximating the pseudo inverse of the forward projection operator Φ_F^0. Let the discrete grid on which the SAR image is formed be $\mathbb{G}_{ml} = (x_m, y_l, 0)$ and the range files $\Delta\mathbf{R}_{mln} = \|\mathbf{r}(\tau_n) - \mathbb{G}_{ml}\| - \|\mathbf{r}(\tau_n)\|$, where $m = \{1,2,...,M\}$, and $l = \{1,2,...,L\}$. The well known matched filter and back projection techniques realise the image formation via $\mathbf{X} = \Phi_B^0(\mathbf{Y}_i)$ in which the backward projection operator Φ_B^0 is the Hermitian transpose of Φ_F^0:

$$X(m,l) = \sum_{k=1}^{K}\sum_{n=1}^{N} Y_i(f_k,\tau_n)\exp\left(\frac{j4\pi f_k \Delta\mathbf{R}_{mln}}{c}\right) \tag{4}$$

Based on the imaging mechanism, multiple targets detection algorithms are valid to mark the ground moving targets in the formed images. In particular, DPCA is implementing the subtractions among the formed SAR images between different channels, ATI is realised by multiplying the formed image from a channel with the conjugate of the complex image from another channel, a compressed sensing based method is exploiting the sparsities pixel-wise in the image domain [5], and a sparse regularised minimisation model is generalising the moving targets and background separation problem as an optimisation framework [6].

In general, these GMTI techniques are all capable of detecting displaced targets in SAR images and estimating their radial velocities. For the rest of the paper, we employ a fast back projection approach [7] to do efficient high-resolution SAR imaging, and the sparsity based optimisation method we previously developed to realise the targets detection and radial velocities estimations [6].

C. Moving Targets Relocations with DEM

Since we can indicate the moving targets in SAR images based on the aforementioned approaches, here we aim to integrate the GMTI outputs and DEM into the SAR imaging algorithm (4). Given the velocity vector $\mathbf{V}_t = (v_t^{(x)}, v_t^{(y)}, v_t^{(z)})$ for a moving target and the subdata $\mathbf{Y}_t$ which corresponds with this target, the image formation of this specific target with DEM can be written as:

$$X_t(m,l) = \sum_{k=1}^{K}\sum_{n=1}^{N} Y_t(f_k,\tau_n)\times \exp\left(\frac{j4\pi f_k(\|\mathbf{r}(\tau_n) - \mathbb{G}'_{ml} - \mathbf{V}_t\tau_n\| - \mathbf{R}_0(\tau_n))}{c}\right) \tag{5}$$

where $\mathbb{G}'_{ml} = (x_m, y_l, z(m,l))$ is the physical grid with the elevation information, the enriched range files $\Delta\mathbf{R}'_{mln} = \|\mathbf{r}(\tau_n) - \mathbb{G}'_{ml} - \mathbf{V}_t\tau_n\| - \mathbf{R}_0(\tau_n)$ contain the DEM and target states, and $\mathbf{R}_0(\tau_n) = \|\mathbf{r}(\tau_n) - \mathbf{r}_{ref}\|$ denotes the distance files with azimuth time between the platform and a reference point $\mathbf{r}_{ref}$. Here the reference point $\mathbf{r}_{ref}$ is the scene center which can incorporate the DEM, and it can be pre-computed as a constant vector.

To be specific, the fast SAR imaging technique [7] operates by splitting the raw data into blocks and calculate the pixel reflectivities in parallel within each data block. The imaging implementation for each block still follows the basic back projection format. Therefore, it is straightforward to utilise the DEM and velocity information in the fast image formation by manipulating the differential range $\Delta\mathbf{R}'_{mln}$ in (5), i.e. incorporating the DEM into $\mathbb{G}'_{ml}$ and $\mathbf{r}_{ref}$, and setting $\Delta\mathbf{R}'_{mln} = \|\mathbf{r}'(\tau_n) - \mathbb{G}'_{ml}\| - \mathbf{R}_0(\tau_n)$ where $\mathbf{r}'(\tau_n) = \mathbf{r}(\tau_n) - \mathbf{V}_t\tau_n$, to achieve moving targets imaging with better relocations. Therefore, the computations remain consistent with (4) in the imaging process and the fast SAR imaging technique [7] still holds.

In a number of scenarios we only have the estimated radial velocities or our emphasis is on the target relocations, the differential range can be approximated via:

$$\begin{aligned}\Delta\mathbf{R}'_{mln} &\cong \|\mathbf{r}(\tau_n) - \mathbb{G}'_{ml}\| + v_t^{(rad)}\tau_n - \mathbf{R}_0(\tau_n) \\ &= \|\mathbf{r}(\tau_n) - \mathbb{G}'_{ml}\| - \mathbf{R}'_0(\tau_n)\end{aligned} \tag{6}$$

where $v_t^{(rad)}$ describes the radial velocity with which the target moves away from the antenna, and the distance files $\mathbf{R}_0(\tau_n)$ can be flexibly replaced with $\mathbf{R}'_0(\tau_n)$ to enforce the radial velocity constraint in moving targets relocations.

D. Moving Target States Estimation

There has been a number of investigations in estimating moving target states/velocities. For example, it is well known that the radial velocities of moving targets correspond to the phase differences between SAR images from different channels in ATI [8][9], and the azimuth velocities can be estimated through bank of filters[10]. It was suggested in [11] that the azimuth velocities of moving targets can be charactered with a Fractional Fourier transform in the time-frequency domain. In [12] it was reported that the estimated velocities can be selected by best focusing the targets to give sharp image patterns and also maintaining the data fidelity.

Here the utilisation of DEM can give us a direct estimation on the $v_t^{(z)}$ in $\mathbf{V}_t$ by differentiating the elevations, which provides us a further constraint on the velocity estimations. It can also be used as an auxiliary criterion to help calibrate the velocities estimated by other methods. Especially when the targets are moving on roads in urban environments, the geometrical information of the road can be used in combination with the DEM to estimate the target states in three directions $(v_t^{(x)}, v_t^{(y)}, v_t^{(z)})$.

IV. EXPERIMENTAL RESULTS

In this section we demonstrate the exploitation of DEM in AFRL GOTCHA data set [13] and compare our estimations to the ground truth data. An X-band SAR system with three Radar channels operates in an urban environment and collects 71 seconds raw data (PRF is 2.17 kHz and the transmitted chip is centred at 9.6 GHz). The original data $\mathbf{Y}_1$, $\mathbf{Y}_2$ and $\mathbf{Y}_3$ were intentionally range-gated from 5400 range samples to 384 range samples for memory considerations. We replace the missing range samples with zeroes and rebuild the complete phase histories $\mathbf{Y}_i \in \mathbb{C}^{5400\times 200}$ where $i = \{1,2,3\}$. Then with the 2D channel balancing technique presented in [4], we keep calibrating the raw phase histories with 8000 azimuth samples and only preserve the 800 calibrated samples in the low frequencies till all data has been processed.

A. DEM Setup

Note that the DEM is absent in the original dataset, we need to extract proper DEM data for the experiments. A coarse DEM on a regular 80×60 grid with latitude and longtitude ranges of 0.0240 and 0.0250 respectively was obtained from the United States Geological Survery (USGS) seamless dataset. The coarse DEM coverage was initially chosen to be larger than the observed scene of our SAR system for further processing.

Since the monitored region does not match the retrieved DEM pair $(\mathbb{G}_{coarse}, \mathbf{E}_{coarse})$ at this stage where $\mathbb{G}_{coarse}$ denotes a grid on the xy-plane (similar to $\mathbb{G}_{ml}$) and $\mathbf{E}_{coarse}$ are the corresponding elevation values, we have to find a reference point $(\mathbb{X}_{ref}, E_{ref})$ so that the elevation map $(\mathbb{G}_{ml}, \mathbf{E}_{ml})$ can be estimated by shifting the $(\mathbb{G}_{coarse}, \mathbf{E}_{coarse})$ based on this point $(\mathbb{X}_{ref}, E_{ref})$, and then interpolating on the imaging grid $\mathbb{G}_{ml}$.

Given that we have the ground truth GPS information of one moving target $(\mathbb{X}_t, \mathbf{E}_t)$, where $\mathbb{X}_t$ contains its xy positioning information and $\mathbf{E}_t$ are the corresponding z coordinates, and they form a path on the terrain surface, the reference point $(\mathbb{X}_{ref}, E_{ref})$ can be estimated by best matching the path to the DEM:

$$\min_{\mathbb{X}_{ref}, E_{ref}} \frac{1}{2}\|\mathbf{E}_t - \Gamma(\mathbb{G}_{coarse} - \mathbb{X}_{ref}, \mathbf{E}_{coarse} - E_{ref}, \mathbb{X}_t)\|_2^2 \tag{7}$$

where $\Gamma(\mathbb{X}_{raw}, \mathbf{Z}_{raw}, \mathbb{X}_{new})$ is the operator to interpolate the surface $(\mathbb{X}_{raw}, \mathbf{Z}_{raw})$ at the query points $\mathbb{X}_{new}$, and return the estimated elevation values.

The interpolated DEM shifted with the reference point is shown in Fig. 2. As shown in the DEM, the monitored region has significant elevation variations.

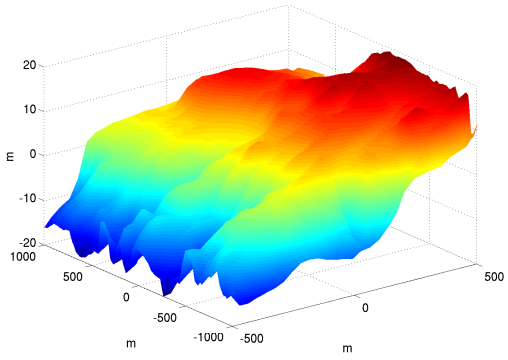

Fig. 2. The estimated DEM which is associated with the imaging grid.

B. Moving Targets Relocations

Given the estimated DEM and pre-processed phase histories, here we focus on the processing of the GOTCHA data from azimuth number 144001 to 146000 and compare the relocations to the ground truth GPS of one moving target. The data is divided into five sub-apertures and each sub-aperture contains 400 azimuth samples.

We first employ the GMTI technique described in [6] and estimate the radial velocities of the moving targets for the five sub-apertures. Here other GMTI techniques which are able to give estimations on radial velocities can also be used. As we have estimated the velocity map for the whole image, the estimated velocities can vary from pixel to pixel and the accuracies of relocations are very sensitive to the estimated radial velocities. Instead of giving a single estimation on the radial velocity, we consider a small 30×30 window around the target for which we have the ground truth, and introduce an estimation bar to give a range for the estimated radial velocity. We denote the minimum/mean/maximum radial velocities in the estimation bar for the $i-$th sub-aperture as $v_i^{(rad,min)}$, $v_i^{(rad,mean)}$ and $v_i^{(rad,max)}$ respectively. In this way we allow certain estimation tolerances for the target radial velocities. These radial velocities can then be used in (5) and (6) to give moving targets relocations. As we now have a range for the estimated radial velocities, this will induce different relocated positions and build up a window to indicate its possible locations. The filled region in Fig. 3 stands for the boundary of all possible target positions.

We extract the five relocated positions of the moving target in five sub-apertures based on the radial velocity estimation bar, and compare the relocated target path to the ground truth GPS. The results can be found in Fig. 3.

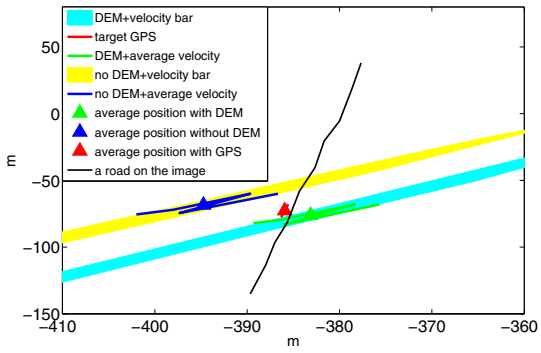

Fig. 3. Comparisons between the ground truth path of the moving target and the relocations (with and without the DEM). The black line indicates the road in the SAR image.

As shown in Fig. 3, the relocated path of the target with DEM (green line) is significantly closer to the ground truth (red line) and the road (black line) than the relocated path without DEM (blue line). As the five sub-apertures correspond to only 1 second during the flight, the ground truth target path is approximately linear. We can therefore compare the average relocated locations of five sub-apertures, i.e. the ones marked with ▲ (green and blue) in Fig. 3, to the ground truth (red triangle). The average relocated positions with and without DEM are deviated from the ground truth for 4.4 m and 9.8 m respectively. The improvement is about the same level as the elevation map.

C. Moving Targets Parameters Estimation

The DEM can be further exploited in the estimation of moving targets velocities. Since the target is likely to move slowly in the z direction, $v_t^{(z)}$ can be estimated by differentiating the positions of the moving target. It gives us an additional constraint on the velocities to help estimate the full state of the target. Particularly in the urban environment, the moving target is likely to move on the roads. The direction of the road gives us another restriction on the velocity estimations. Furthermore, the velocity estimations can be calibrated by allowing errors in radial velocity estimations, i.e. relocating the moving target to the intersection of the road and its possible locations (the filled region in Fig. 3). Calibrated relocated positions of the target give us calibrated radial velocity estimations and therefore promote the accuracy of the estimated radial velocity.

Here we first calibrate the radial velocity estimations. The estimated radial velocity of the target $v_t^{(rad)}$ is adjusted to relocate the moving target to the road (black line). Based on the road direction in the formed image, we can approximately leverage this equation $v_t^{(y)} = 14.1 \times v_t^{(x)}$. Then its velocity in z direction $v_t^{(z)}$ can be estimated by differentiating its relocated positions. The accuracy on estimating $v_t^{(z)}$ is thus limited by the accuracy of the DEM. Specifically, with the normalised vector in radial direction $\mathbf{n}^{(rad)}$ which goes from the target to the platform, the $(v_t^{(x)}, v_t^{(y)}, v_t^{(z)})$ and $v_t^{(rad)}$ follow this

TABLE I
COMPARISONS BETWEEN THE GROUND TRUTH AND ESTIMATIONS

sub-aperture number	1	2	3	4	5
estimated $v_t^{(x)}$ (m/s)	0.88	0.9	0.94	0.95	1.0
ground truth $v_t^{(x)}$ (m/s)	0.99	1.03	1.07	1.1	1.14
estimated $v_t^{(y)}$ (m/s)	12.4	12.72	13.2	13.4	14.1
ground truth $v_t^{(y)}$ (m/s)	12.9	13.1	13.3	13.5	13.7
estimated $v_t^{(z)}$ (m/s)	0.1	0.12	0.2	0.17	0.38
ground truth $v_t^{(z)}$ (m/s)	0.32	0.28	0.25	0.21	0.2

restriction:

$$v_t^{(rad)} = v_t^{(x)}\langle \mathbf{u}_x, \mathbf{n}^{(rad)} \rangle + v_t^{(y)}\langle \mathbf{u}_y, \mathbf{n}^{(rad)} \rangle + v_t^{(z)}\langle \mathbf{u}_z, \mathbf{n}^{(rad)} \rangle \tag{8}$$

where $\mathbf{u}_x$, $\mathbf{u}_y$ and $\mathbf{u}_z$ are the unit vectors in x, y and z directions respectively, $\langle \cdot, \cdot \rangle$ is the dot product operator.

Based on (8), we can estimate the target velocities $(v_t^{(x)}, v_t^{(y)}, v_t^{(z)})$. We compare our estimations to the ground truth and show the results in Table I. It can be seen that the estimations on the target velocities match the ground truth with high accuracies. In practice, the geometrical information and DEM can be used as the auxiliary restrictions on other velocity estimation approaches to give SAR/GMTI applications better robustness.

V. CONCLUSION

This paper presents a work for relocating moving targets and estimating targets' states with DEM in SAR/GMTI scenarios. Specifically by modeling the DEM in the SAR imaging and moving targets relocation scheme, the positioning of the moving targets can be further improved. Also the DEM can give us rough estimations on the z direction velocities, and it can be combined with geometrical information especially in urban environments to give further criteria to calibrate velocity estimations. The experimental results based on the GOTCHA GMTI dataset illustrate the effectiveness of the presented processings.

ACKNOWLEDGMENT

This work was supported by the Engineering and Physical Sciences Research Council (EPSRC) grants [EP/K014277/1]; and the University Defence Research Collaboration (UDRC) in Signal Processing.

REFERENCES

[1] S. Chiu and C. Livingstone, "A comparison of displaced phase centre antenna and along-track interferometry techniques for RADARSAT-2 ground moving target indication," *Canadian Journal of Remote Sensing*, vol. 31, no. 1, pp. 37–51, 2005.

[2] I. Sikaneta and C. Gierull, "Ground moving target detection for along-track interferometric SAR data," in *Aerospace Conference, 2004. Proceedings. 2004 IEEE*, vol. 4, March 2004, pp. 2227–2235 Vol.4.

[3] J. Ward, "Space-time adaptive processing for airborne radar," in *Space-Time Adaptive Processing (Ref. No. 1998/241), IEE Colloquium on*, Apr 1998, pp. 2/1–2/6.

[4] C. Gierull, "Digital channel balancing of along-track interferometric SAR data," in *Technical Memorandum DRDC Ottawa TM 2003-024*. Defence R&D, Ottawa, Canada, March 2003.

[5] L. Prunte, "GMTI from multichannel SAR images using compressed sensing," in *Synthetic Aperture Radar, 2012. EUSAR. 9th European Conference on*, April 2012, pp. 199–202.

[6] D. Wu, M. Yaghoobi, and M. Davies, "A new approach to moving targets and background separation in multi-channel SAR," in *2016 IEEE Radar Conference*, 2016.

[7] S. Kelly and M. Davies, "A fast decimation-in-image back-projection algorithm for SAR," in *Radar Conference, 2014 IEEE*, May 2014, pp. 1046–1051.

[8] R. M. Goldstein and H. Zebker, "Interferometric radar measurement of ocean surface currents," 1987.

[9] A. Budillon, V. Pascazio, and G. Schirinzi, "Amplitude/phase approach for target velocity estimation in AT-InSAR systems," in *2008 IEEE Radar Conference*, May 2008, pp. 1–5.

[10] G. Palubinskas, F. Meyer, H. Runge, P. Reinartz, R. Scheiber, and R. Bamler, "Estimation of along-track velocity of road vehicles in sar data," in *Remote Sensing*. International Society for Optics and Photonics, 2005, pp. 59 820T–59 820T.

[11] S. Chiu, "Application of fractional fourier transform to moving target indication via along-track interferometry," *EURASIP Journal on Advances in Signal Processing*, vol. 2005, no. 20, pp. 1–11, 2005.

[12] D. Wu, M. Yaghoobi, and M. Davies, "Sparsity based ground moving target imaging via multi-channel SAR," in *Sensor Signal Processing for Defence (SSPD), 2015*, Sept 2015, pp. 1–5.

[13] S. M. Scarborough, C. H. Casteel, Jr., L. Gorham, M. J. Minardi, U. K. Majumder, M. G. Judge, E. Zelnio, M. Bryant, H. Nichols, and D. Page, "A challenge problem for SAR-based GMTI in urban environments," *Proc. SPIE*, vol. 7337, pp. 73 370G–73 370G–10, 2009.